Journal of GeoEngineering, Vol. 18, No. 3, pp. 129-143, September 2023
http://dx.doi.org/10.6310/jog.202309_18(3).4

EFFECTIVENESS OF NEAR SURFACE GROUND IMPROVEMENT AROUND PILED-RAFT FOUNDATION IN WEAK SOIL BASED ON ANALYTICAL DESIGN AND FINITE ELEMENT MODELING

Nadarajah Ravichandran [1*] and Siddharth Marathe [2]

ABSTRACT

Taller wind turbines are preferred to access high and steady wind at a higher altitude to increase the efficiency of a wind turbine, but they require an extensive foundation, particularly when subsurface soil has poor engineering properties. One of the solutions to this problem is to improve the engineering properties of the poor near-surface ground to gain a net economic advantage for foundation construction. In this study, the effectiveness of the ground improvement around piled-raft foundation in weak soil is investigated using analytical and three-dimensional finite element (FE) methods. Five different ground improvement depths from 2.0 m to 3.6 m and radii from 6 to 15 m were considered to develop a relationship between the geometry of ground improvement, the performance of the foundation, and the cost of the foundation. The analytical analysis shows that the pile length required to meet the safety and serviceability requirements decreased from 48.4 m in the unimproved soil to 9.85 m in the 3.6 m improved soil, resulting in a 33.5% cost reduction. The cost-benefit for various depths of ground improvement shows a nonlinear variation, indicating that the most economical depth of ground improvement is within the range considered in this study. The finite element modeling was conducted using ABAQUS with frictional contacts at the soil-pile and raft-pile interfaces to capture the load transfer accurately. The ABAQUS results were much lower than the analytical results for the linear elastic and elastoplastic constitutive models.

Key words: wind turbine foundation, piled-raft foundation, ground improvement, finite element analysis.

1. INTRODUCTION

Energy consumption has grown in the US and worldwide over the decades; thus, energy demand has increased rapidly. Sustainable options to meet these demands have become particularly important in maintaining the health of the planet and humanity. Among the many, the contribution of wind, solar, biomass, and geothermal energy sources to the global energy demand is shown in Fig. 1. The figure shows that wind energy has been gaining momentum and is predicted to continue to increase. Taller wind turbines are constructed to capture the steadier and stronger wind at higher altitudes to increase the efficiency of each wind turbine. Reports show that the annual energy production increases by 0.5% to 1.0% with every meter increase in the wind turbine height (Lantz 2019). However, as the wind turbine height increases, the size and cost of the foundation that supports the turbine also increase. As the foundation is the most important component for supporting the above-ground structures, the design and construction of the foundation are crucial to maintaining the overall stability of the above-ground structures. The size of the foundation is not only dictated by the height of the wind turbine but also by the engineering properties of the subsurface soil and their variability.

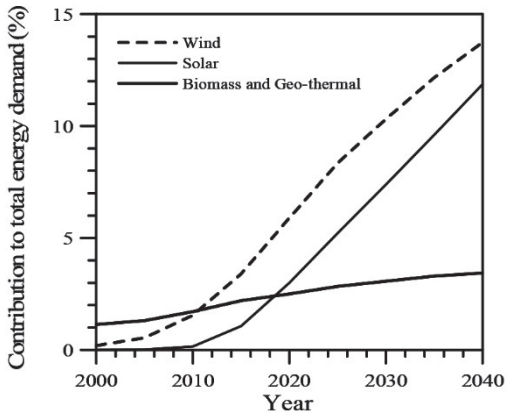

Fig. 1 Global renewable energy forecast (data source: US EIA)

Securing areas with favorable wind and subsurface conditions for building taller wind turbines is challenging. A significantly large foundation may be required to support taller wind turbines at sites where the subsurface soil has poor engineering properties. A high upfront foundation cost may result in an uneconomical wind farm project. In such a situation, the poor insitu soil may be improved using a suitable ground improvement technique to improve the engineering properties of the subsurface soil around the foundation. The ground modification may not only improve the axial capacity but also the lateral capacity that is critical for resisting large moments induced at the base of the tower. Taghavi *et al.* (2015) investigated the effectiveness of ground improvement on the lateral capacity of pile groups using centrifuge model tests. In their test, the ground was modified using Cement Deep Soil

Manuscript received March 2, 2023; revised June 1, 2023; accepted June 21, 2023.
[1*] Associate Professor (corresponding author), Glenn Department of Civil Engineering, Clemson University, 202 Lowry Hall, Clemson, SC 29634 (e-mail: alizakariyast@mail.ugm.ac.id).
[2] Graduate Student, Glenn Department of Civil Engineering, Clemson University, 202 Lowry Hall, Clemson, SC 29634.

Mixing (CDSM) method. Yamashita *et al.* (2012) conducted a field test to investigate the seismic behavior of a building supported on a piled-raft foundation with ground improvement. In their study, the ground was modified in a grid form using deep cement mixing walls.

In general, raft, pile group, or piled-raft foundations is chosen to support wind turbines. Ravichandran and Shrestha (2018) performed comprehensive analytical design, finite element modeling, and multi-objective optimization of these three commonly used foundation types. They concluded that the piled-raft foundation is the most economical for supporting tall wind turbines in weak clayey soils. In weak subsurface soil, a large diameter raft supported by many long piles was required to meet the safety and serviceability design requirements. Melese (2022) investigated the performance of piled-raft foundations using the finite element method with a granular layer (cushion) beneath the raft to disconnect the pile from the raft. From the study, it was concluded that for small piled rafts, nonconnected piled rafts show less stiffness than connected piled rafts, and the soil is highly stressed and shows greater raft settlement. Pham *et al.* (2018) analyzed a case study to compare the performance of piled-raft and raft foundations supporting tall wind turbines in soft compressible soil with and without ground improvement using 3D finite difference program, FLAC. They concluded that there was a significant decrease in the total and differential settlements for piled-raft compared with the raft case. Also, the soil settlements, the foundation rotation, the axial forces, and the bending moments exerted on the reinforcements decreased when the area improvement ratio increased. Gaihre (2020) conducted a similar study using the 3D finite element program PLAXIS 3D and also found a significant decrease in the total and differential settlements for piled-raft as compared to the raft case.

The analytical design procedures currently available in the literature to perform the geotechnical design of pile-raft foundations have limitations, particularly when the ground is improved with finite depth and width. In such situations, a three-dimensional (3-D) finite element method can be used to design and analyze the foundation. In this study, the effectiveness in terms of performance and cost of modifying the near-surface soil around a piled-raft foundation was investigated using analytical and 3-D finite element methods. The total cost and the performance in terms of settlements before and after the ground modifications were compared. The design and analysis procedures and results are presented in the subsequent sections.

2. SAMPLE WIND TURBINE AND SITE CONDITION

2.1 Wind Turbine Specifications and Design Requirements

The effectiveness of improving the ground around the piled-raft foundation was demonstrated by considering a wind turbine with a height of 80 m and a base diameter of 6.75 m. These dimensions and other parameters of the wind turbine were obtained from Lyrner *et al.* (2010). The pile length was adjusted to meet the design requirements while keeping the diameter of the raft and the number of piles constant to reduce the number of design variables. A safety factor of 2.5 was considered adequate for safety checks. For the serviceability requirement, the vertical misalignment of 3 mm/m of the tower height was considered acceptable against tower rotation (Grunberg and Gohlmann 2013). This yielded an allowable differential settlement of 24 mm and a rotation of 0.171° for the tower height of 80 m considered in this study.

2.2 Properties of Insitu and Improved Soil

The insitu soil is a homogeneous soft clay suitable for modification using cement soil mixing (CSM). The engineering properties of the clay were obtained from Quiroga *et al.* (2017). The key properties of the insitu and improved soils are listed in Tables 1 and 2, respectively. It should be noted that the soft clay considered in this study was used as part of a geotechnical centrifuge experimental study to investigate the ground improvement against earthquake loads (Quiroga *et al.* 2017). The stress-strain curves of the insitu and improved soils are shown in Figs. 2(a) and 2(b), respectively. Figure 2 shows that the strength and deformation (modulus) properties of the improved clay are significantly higher than that of unimproved insitu soil. The elastic modulus and undrained shear strength of the improved clay were calculated as 120,000 kPa and 360 kPa, respectively. These values are 394% and 878% higher than that of unimproved insitu soil. The unimproved and improved clay yield strengths are approximately 90 kPa and 720 kPa, respectively. These observations indicate that the improved soil will have a higher bearing capacity and lower settlement or shorter piles to meet the safety and serviceability requirements of the piled-raft foundation.

The analytical design procedures available in the literature are incapable of incorporating the limited extent of the ground improvement in the horizontal direction. Therefore, the geotechnical designs were performed by assuming that the ground improvement extended infinitely in the horizontal direction ($R = \infty$). With a ground improvement, the supporting soil profile becomes a two-layered soil with an improved layer above the insitu soil. A total of five different depths (V_i, i = 1, 2, …, 5) of improvement were considered, as shown in Fig. 3, to develop a relationship between the depth of ground improvement and the performance and cost of the foundation. The 2.0 m (V_1), 2.4 m (V_2), 2.8 m (V_3), 3.2 m (V_4), and 3.6 m (V_5) of the depth of ground improvement were considered. These depths are 0.25, 0.3, 0.35, 0.4, and 0.45 times the diameter of the raft, respectively. The radius of ground improvement

Table 1 Properties of in situ clay (unimproved)

Geotechnical Properties	Values
Saturated unit weight (kN/m^3)	19.20
Liquid limit (%)	32
Plastic limit (%)	17
Specific gravity	2.69
Average water content (%)	22
Young's modulus (kPa)	30,500
Undrained shear strength (kPa)	41

Table 2 Mix design and properties of improved soil

Mix Design Properties	Values
Water to cement ratio	1
Cement content (%)	10
Cement factor	270
Total water to cement ratio	4.4
Young's modulus (kPa)	120,000
Undrained shear strength (kPa)	360

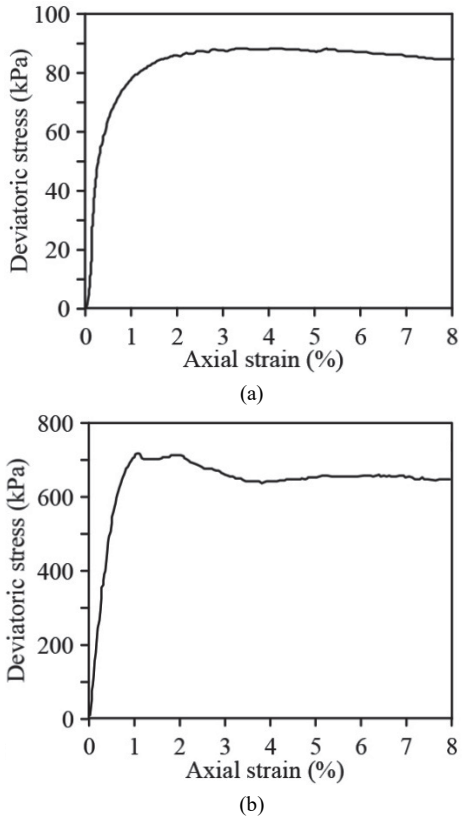

Fig. 2 Measured stress-strain behavior from consolidated undrained compression test (recreated from Quiroga *et al.* 2017) (a) unimproved clay and (b) CSM improved clay

(R_i) for each depth was assumed to be the radius of the raft (R_R) plus the depth of improvement (V_i), as shown in Fig. 3. In other words, the improved ground is a cylinder with a height of V_i and a radius of $R_R + V_i$.

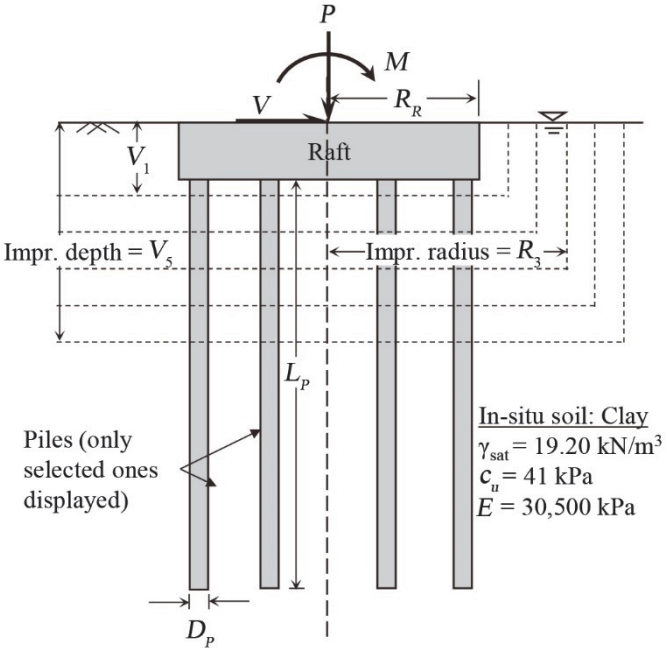

Fig. 3 Piled-raft foundation and with ground improvement scheme (not to scale)

3. ANALYTICAL DESIGN OF PILED-RAFT FOUNDATION

3.1 Design Loads

The total vertical load (P) was calculated by adding the weight of the tower and other above-ground components of the wind turbine, such as the nacelle and rotor. The final vertical load was computed to be 8,819.19 kN. For a design wind speed of 80 mph, the wind load was calculated according to ASCE 7-10 (ASCE 2010). Since the wind speed increases from the ground surface nonlinearly, the tower was divided into several segments, and the drag force on each section was calculated considering the corresponding wind speed. The bending moment was calculated by multiplying the horizontal force on each tower segment and other components by the corresponding height from the bottom of the tower. The total horizontal load (V) and bending moment (M) were estimated to be 579.49 kN and 30,223.70 kN·m, respectively.

3.2 Geotechnical Design for the Safety of the Wind Turbine System

3.2.1 Design for Vertical Load

The total vertical load capacity of the piled-raft foundation is the summation of the vertical capacities of the raft and the piles. The vertical load capacity of the raft was computed as the product of the raft area and the ultimate bearing capacity of the raft. The axial load capacity of the piles was computed by using the method outlined in O'Neil and Reese (1999). Then, the assumed foundation dimensions in the unimproved soil resulted in a factor of safety of 2.8, which is slightly greater than the design minimum vertical load factor of safety of 2.5. The details of the analytical design procedure can be found in Ravichandran and Shrestha (2018) and Shrestha and Ravichandran (2017). For the piled-raft in the improved section of the ground, the vertical load capacity was computed using similar procedures with appropriate soil properties for the raft and piles.

3.2.2 Design for Moment Load

The moment load capacity of the piled-raft foundation was computed following the method outlined in Hemsley (2000). The total moment load capacity of the piled-raft foundation was calculated by adding the individual moment load capacities of the piles and the raft. Then, the moment load capacity of the piled-raft foundation, considering the soil-foundation system as a single block, was calculated. The moment load capacity of the piled-raft is the smallest of the two capacities. For the assumed dimensions, load, and soil conditions, it was found that the sum of the individual component capacity was the smallest and thus considered as the moment load capacity of the piled-raft foundation. This process was repeated by adjusting the foundation dimensions until the minimum design factor of safety of 2.5 for the moment capacity was achieved. The details of the analytical design procedure can be found in Ravichandran and Shrestha (2018) and Shrestha and Ravichandran (2017). The foundation design in the improved soil was performed following similar procedures with appropriate soil properties. However, the moment load capacity governed the final design for unimproved soil conditions, whereas the differential settlement controlled the final design for the improved soil conditions.

3.2.3 Design for Horizontal Load

The horizontal load capacity of piles was calculated using the procedure outlined in Brom (1964). Although this method is primarily developed for the horizontal deflection of a single pile, it was still used by assuming that the deflection behavior of the pile in a piled-raft foundation is similar to that of a single pile. It should also be noted that there is no well-defined analytical method for calculating the horizontal deflection of piled-raft foundation. For the dimensions obtained from the moment load capacity check, the horizontal load capacity of a single pile was estimated to be 342.51 kN, and the corresponding horizontal deflection to be 4.69 mm for the unimproved soil condition. The safety factor against the horizontal load was calculated to be 15.40 for the foundation dimensions required for meeting the moment load capacity discussed in the previous section. The details of the analytical design procedure can be found in Ravichandran and Shrestha (2018) and Shrestha and Ravichandran (2017).

Calculation of the horizontal deflection of the piled-raft foundation in a two-layered soil profile, with an upper layer of improved soil and a lower layer of unimproved soil, is complex and challenging. In this paper, the deflection of a pile with its entire length in improved soil was calculated and compared to a pile deflection in unimproved soil. Then, the deflection of the pile embedded in a two-layered soil profile was estimated by taking the weighted average of the deflections in unimproved and improved soils. This was repeated for each soil improvement depth, with the depth of improvement determining the weight of each soil in each case's respective deflection averages.

3.2.4 Determination of Vertical Load-Settlement Response

The vertical settlement of the piled-raft was calculated using the method proposed by Randolph (1994). This method calculates the vertical settlement by load sharing between the raft and the pile. The percentage of the load carried by the raft and the stiffness of the piled-raft foundation were calculated using Eqs. (1) and (2) proposed by Randolph (1994).

$$K_{pr} = \frac{K_p + (1 - 2\alpha_{rp})K_r}{1 - \alpha_{rp}^2 (K_r / K_p)} \tag{1}$$

$$\frac{P_r}{P_r + P_p} = \frac{(1 - \alpha_{rp})K_r}{K_p + (1 - 2\alpha_{rp})K_r} = X \tag{2}$$

where P_r is the load carried by the raft, P_p is the load carried by the piles, K_r is the stiffness of raft, K_p is the stiffness of the pile group, K_{pr} is the stiffness of the piled-raft foundation, and α_{rp} is the pile-raft interaction factor. The pile-raft interaction factor α_{rp} varies between 0.65 and 0.8, depending on pile spacing and the slenderness ratio. However, Clancy and Randolph (1996) suggested that for a larger pile group, the interaction factor is independent of the slenderness ratio and pile spacing and tends to have a constant value of 0.8. The required piled-raft stiffness was calculated by dividing the total vertical load by the allowable vertical settlement. The stiffness of the pile is back-calculated by replacing the value of K_{pr} in Eq. (1) and solving the quadratic form of the simplified equation. The ratio of the load carried by the raft is then calculated by using Eq. (2). The stiffness of the piled-raft subjected to vertical load will continue to be active until the pile's load-bearing capacity is entirely mobilized at load P_A, as shown in Eq. (3).

$$\text{For } P \le P_A \quad S = \frac{P}{K_{pr}}$$

$$\text{For } P > P_A \quad S = \frac{P_A}{K_{pr}} + \frac{P - P_A}{K_r} \tag{3}$$

The allowable vertical settlement of the piled-raft foundation in unimproved soil for a vertical design load of 8.81 MN was calculated to be 30 mm. The design load is lower than the allowable load P_A, indicating that the pile capacity is not fully mobilized. Thus, both piles and rafts contribute to resisting the applied load. A 9.87 mm vertical settlement was predicted for the vertical design load of 8.81 MN. It was also predicted that the raft carried 40.03% of the vertical load, and the piles carried the rest in the unimproved soil case.

A similar procedure was adopted to calculate the vertical load-settlement behavior of the foundation in the improved soil condition with respective soil properties. The equivalent modulus of elasticity and the undrained shear strength were computed using a weighted average method (Das 2019).

3.2.5 Design for Differential Settlement and Rotation

The calculation of differential settlement is critical for the foundation of tall wind turbines because a small differential settlement can cause significant eccentricity in the above-ground component that may result in a complete collapse of the wind turbine. Since the piled-raft foundation has a rigid raft supported by several piles, the load transfer between piles and raft must be computed to calculate the rotation or differential settlement of the piled-raft foundation system. The differential settlement calculation procedure proposed by Shrestha *et al.* (2018) was adopted in this study. In their method, the total bending moment is divided randomly between the raft and the piles and adjusted until the differential settlement profiles of the piles and raft are matched in the plane of the bending, as shown in Fig. 4. The calculation of the differential settlement of raft and piles is discussed below.

3.2.6 Differential Settlement Profile of Raft

The differential settlement and the rotation of the tower are caused by the horizontal force exerted by the wind on the above-ground components. In this study, the rotation of the raft was calculated using Eq. (4), given by Grunberg and Gohlmann (2013).

$$\theta = \frac{M_{\text{found}}}{c_s I_{\text{found}}};\ c_s = \frac{E_s}{f' \sqrt{A_{\text{found}}}} \tag{4}$$

where c_s is the foundation modulus, M_{found} is the fixed-end moment at the soil-structure interface, E_s is the modulus of elasticity of soil, I_{found} is the second moment of inertia for the area of the foundation given by A_{found}, and f' is the shape factor for overturning whose value is taken as 0.25 (Grunberg and Gohlmann 2013). A trigonometric relationship between the rotation (θ) and the radius was used to calculate the differential settlement of the raft.

3.2.7 Differential Settlement Profile of Piles

To calculate the differential settlement of the pile group, the portion of the bending moment carried by the piles was converted

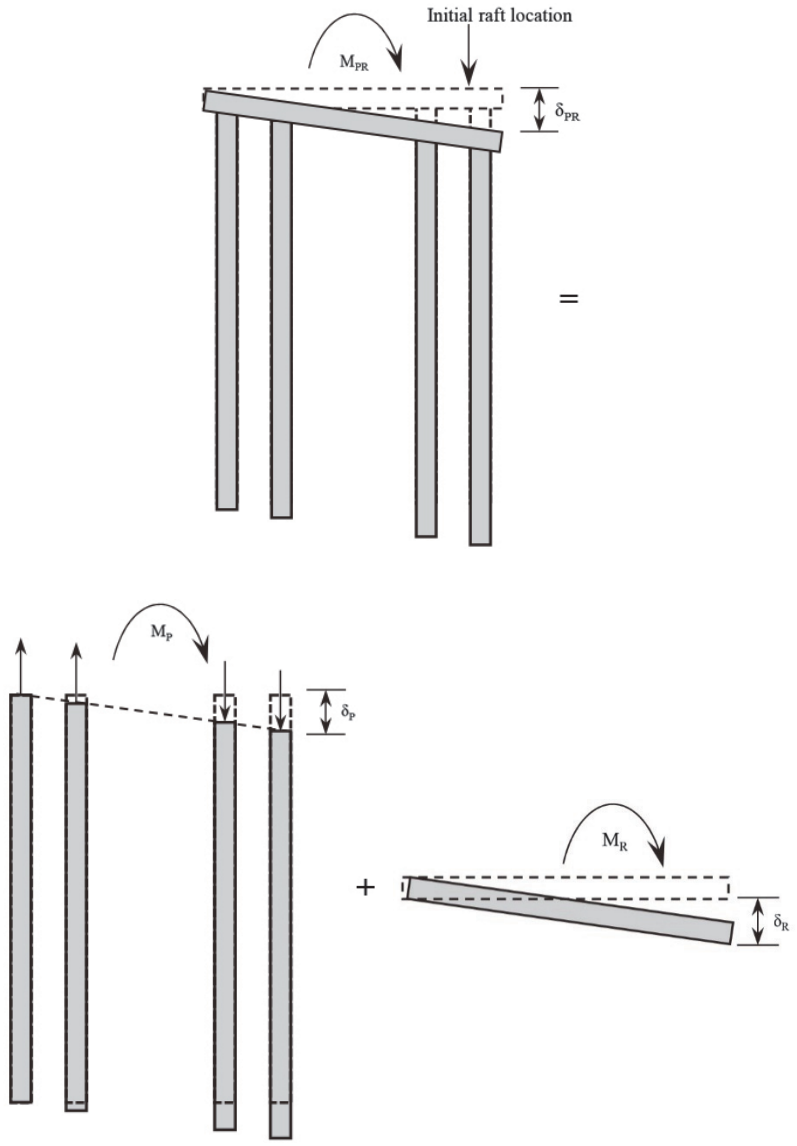

Fig. 4 Distribution of moment and differential settlement calculation procedure

into an equivalent vertical load on each pile based on the relative location of the pile with respect to the center in the plane of the bending moment. Then, the method proposed by Fellenius (1999) was used to calculate the settlement of each pile. This process was reiterated by varying the bending moments shared by the raft and the piles until the settlement profiles of the piles and raft matched. The last settlement profile was considered as the settlement profile of the piled-raft foundation system. For the problem considered in this study, it was found that the raft and piles carried 80.62% and 19.38% of the total bending, respectively, for the foundation in the unimproved soil. The differential settlement of the piled-raft system was 13.80 mm, which gives a rotation of 0.098°. For the 80 m tower height, a rotation of 0.098° will result in a horizontal displacement of 138.05 mm at the top of the tower, which is within the acceptable limit.

3.3 Final Design Outcome

The above design checks resulted in an 8.0 m diameter and 1.0 m thick raft flushed with the ground supported by 24 piles to meet the design requirements in the insitu soil. The piles are 48.4 m long with an outside diameter of 457 mm. These 24 piles were arranged on two circumferences with 3.37 m and 2.23 m diameters, as shown in Fig. 5. For the design in improved near-surface soil, only the lengths of the piles were varied while keeping the other parameters constant.

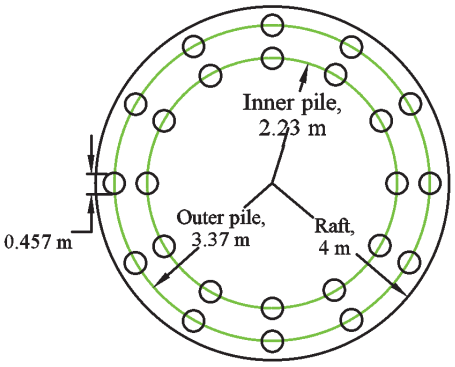

Fig. 5 Plan view of raft and pile arrangement

4. FINITE ELEMENT MODELING OF SOIL-PILE-RAFT SYSTEM

The existing analytical procedures have limitations in accurately designing the piled-raft foundations under complex geometric and loading conditions. Therefore, to gain further insight into the performance with a realistic ground improvement approach, the 3-D FE method could be used.

4.1 Simulation Domain and Boundary Condition

The analytical design outcomes (size, number, length, and location of the piles, size of the raft, and thickness of soil layers) were used to build 3-D FE models for each ground improvement geometry in ABAQUS v2018. ABAQUS has advanced features for accurately representing the soil, pile, raft, soil-pile interface, soil-raft interface, and loading conditions. Separate finite element models were created for each ground improvement depth and analyzed. Each component of the pile-raft-soil system was created and assembled using the assembly module to form the soil-raft-pile system. For accurately modeling soil-pile and soil-raft interaction, the soil was numerically excavated (cored) using the cut instance module in ABAQUS before assembling the components. The numerical coring created space for raft and piles in the soil component. Figure 6 shows the pile-raft assembly and soil domain with space to install the piled-raft foundation numerically. After assembling the components, standard displacement boundary conditions were applied to the vertical and bottom horizontal boundaries of the simulation domain. That is, the horizontal movement of the vertical boundaries (nodes) was restricted in the horizontal direction and allowed movement in the vertical direction. Also, the base (bottom) was fixed in all directions. Figure 7 shows the 3-D FE simulation domain for V1H1 case with proposed boundary conditions.

4.2 Finite Element Mesh Generation

The simulation domain, including the soil, pile, and raft, was spatially discretized using a linear eight-noded hexahedral brick element (C3D8R). Several partitioning techniques available in ABAQUS were used to divide different parts to create a mesh with

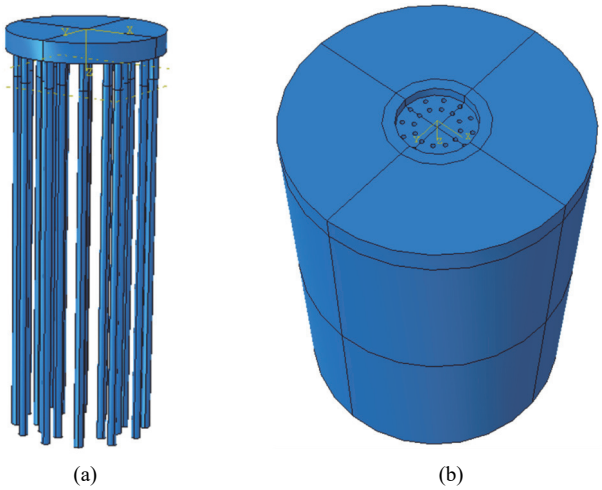

(a) (b)

Fig. 6 Finite element model development: (a) piles and raft assembly and (b) soil domain with space to assemble piled-raft

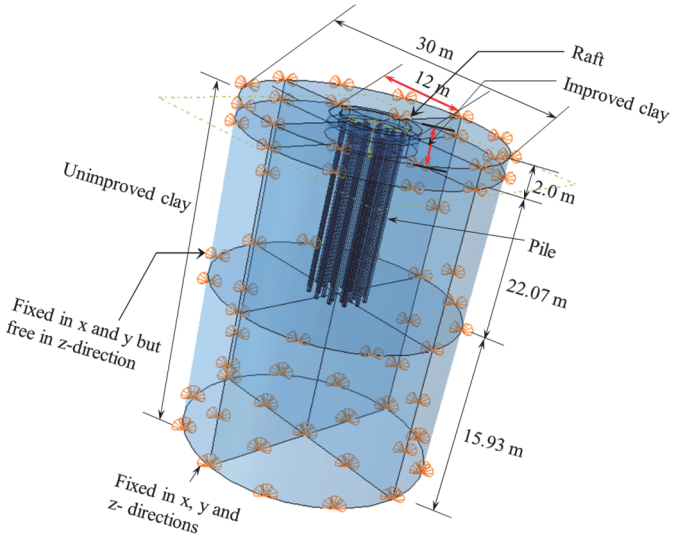

Fig. 7 A 3D simulation domain of piled-raft foundation for an improved ground (V_1H_1)

suitable nodes at the soil-pile, soil-raft, and raft-pile contacts. A coarser mesh was used in the areas where lower stress and/or deformation concentration is expected. A finer mesh was used near the soil-pile and soil-raft interfaces to accurately capture the stress and/or deformation gradient. After selecting the size and mesh refinement areas, size and mesh sensitivity studies were conducted by applying a combined load to ensure the size of the simulation domain and mesh size do not influence the computed responses. This resulted in a cylindrical simulation domain with a diameter of 30 m and a height of 60 m, a finite element mesh with 705,898 nodes, and 638,224 3-D elements. The partition of the simulation domain and the final FE mesh are shown in Fig. 8.

4.3 Soil-Structure Interaction Model

The load transfers at the soil-pile and soil-raft were defined in normal and tangential directions. The normal contact between the pile skin and soil was defined using the "hard" contact module, in which the contact is defined using the master-slave concept, where the stiffer surface is defined as a master surface and the

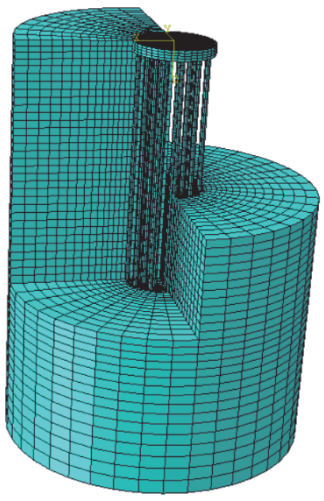

Fig. 8 Finite element mesh and cut sections of soil-pile-raft system

softer as the slave surface. The "hard" contact concept eliminates the penetration of the slave surface into the master surface at constrained locations during iterations. The tangential behavior at the contacts was defined using the friction formulation, also called penalty formulation in ABAQUS. In this formulation, the surfaces in contact can slip relative to each other if the load exceeds its capacity. The frictional capacity at the interface was defined using the friction coefficient, δ. The δ for the pile-unimproved soil and pile-improved soil interfaces were assumed to be 0.35 and 0.45, respectively (NFEC DM 7.02, 1986). The contacts between the top surface of the pile and bottom of the raft, pile toe and soil, and raft and soil were characterized by a surface-to-surface tie constraint. Such tie constraint also utilizes the master-slave concept. The tie constraint binds the two surfaces in contact and thus enables equal translation and rotation between the surfaces in contact throughout the simulation.

4.4 Soil Constitutive Models and Model Parameters

Both linear elastic (LE) and elastoplastic (EP) Drucker Prager (DP) constitutive models were used to represent the soil, and the results were compared. The LE model is a numerically stable and simple model with well-defined input parameters, but it does not represent the soil behavior accurately for the range of strain experienced by the soil. To capture the soil behavior accurately, a nonlinear elastoplastic model can be used. Among the many nonlinear elastoplastic models available in the literature, the DP model was used because it is numerically stable in nonlinear finite element analysis and also captures the nonlinear modulus reduction with strain reasonably well. Since the analytical design procedure is based on elastic theory, the finite element models with LE constitutive model were first analyzed for comparison purposes. Figure 9 shows the yield surface criterion for the DP model and compares it with that of a linear elastic perfectly plastic Mohr-Coulomb model. The LE and EP model parameters are shown in Table 3. One of the key inputs for the EP-DP model is the yield stress versus plastic strain curve. The yield stress (Δσ) was determined from the stress-strain curve as the deviator stress at which the soil exhibited nonlinear behavior. The corresponding plastic strain (ε^p) was calculated by subtracting the elastic strain (ε^e) from the total strain. The value of ε^e at different stress levels were calculated by

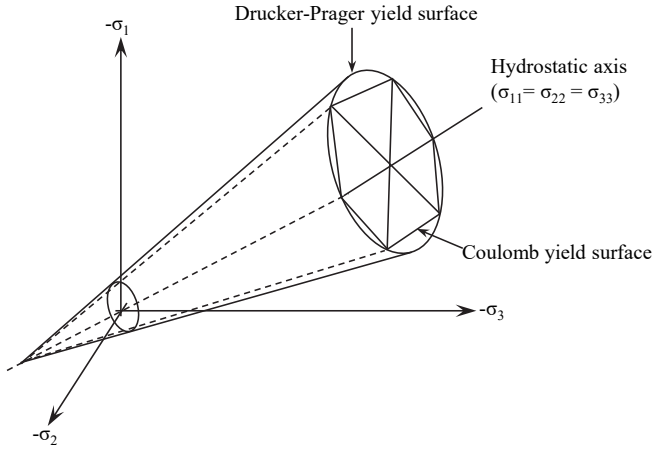

Fig. 9 Schematic representation of DP and MC models and yield surfaces

Table 3 Linear elastic and elastoplastic soil model parameters

Model Type	Parameter	Value
Linear elastic	Density (kg/m^3)	1835.5
	Young's modulus (N/m^2)	3.05×10^7
	Poisson's ratio	0.3
Elastoplastic DP	Shear criterion	Linear
	Flow potential eccentricity	0.1
	Friction angle (°)	0
	Flow stress ratio	1

dividing the initial yield stress Δσ by the initial modulus of elasticity E_0 (*i.e.,* $\varepsilon^e = \Delta\sigma/E_0$). The yield stress versus plastic strain curves for the insitu and improved soils are shown in Figs. 10(a) and 10(b), respectively. From the figures, it can be seen that the yield stress values of the improved clay are significantly higher than that of unimproved insitu soil.

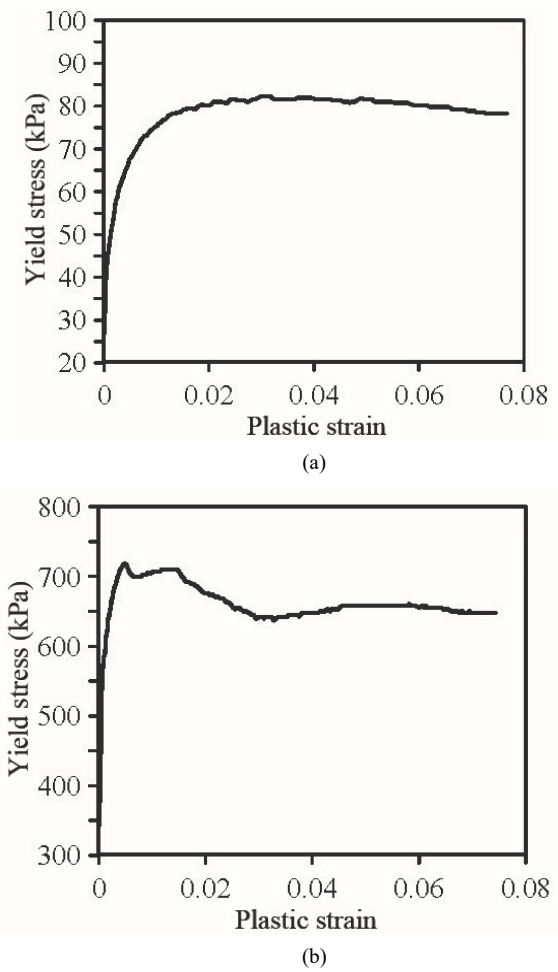

Fig. 10 Elastoplastic DP-H model yield stress vs. plastic strain curve for (a) in situ clay and (b) improved clay

4.5 Pile Constitutive Model and Model Parameters

The piles and raft were assumed to be made of reinforced concrete, and their stress-strain behaviors were represented by a linear elastic model. The density, Poisson ratio, and the elastic modulus of the pile and raft were assumed to be 2549.3 kg/m^3, 0.15, and 3.0×10^{10} N/m^2, respectively.

4.6 Finite Element Analysis

The analysis consisted of three phases: (a) the initial phase, (b) the geostatic phase, and (c) the loading phase. The boundary conditions, contact constraints, and interactions were activated in the initial phase and propagated to the subsequent phases. The initial stresses were calculated in the geostatic phase. The simulations were conducted using the Clemson University Palmetto cluster, a network of high-performance computers. A total of 132 finite element models were created and analyzed in this study under three cases, as detailed below.

Case I: 60 models (30 LE and 30 EP) were created to investigate the effectiveness of ground improvement. In these models, the pile length was varied to meet the design requirements for each improvement depth. For each ground improvement depth (V), six horizontal improvement distances (H) with the same length of piles were considered to determine the effect of improvement in the horizontal direction. The radii of horizontal improvement (R_i, i = 1 to 6) were 6.0, 6.4, 6.8, 7.2, 7.6, and 15 m, respectively, from the center of the raft. The horizontal ground improvement radius of 15 m (H_6) extends to the model's boundary to simulate the analytical design condition (infinite).

Case II: 60 models (30 LE and 30 EP) were created to investigate the performance enhancement of piled-raft foundations with ground improvement. In these models, the pile length was kept the same as that in unimproved (insitu) ground (L_p = 48.4 m). Six horizontal improvement distances, as in Case I, were considered for each ground improvement depth to understand the influence of improvement in the horizontal direction.

Case III: A parametric study was performed by changing the undrained shear strength (s_u) of insitu and improved soils by ±1σ (standard deviation) from the mean s_u(μ). Since the model with the mean shear strength was already created for Case I, 12 additional models were created (6 with μ − 1σ) and 6 with μ + 1σ).

5. COMPARISON OF ANALYTICAL AND FINITE ELEMENT ANALYSES RESULTS

Since the extent of improvement in the horizontal direction was not considered in the analytical design, for one-to-one comparison between the analytical and FE methods, the FE results from the model that extended the ground improvement to the model's boundary (H_6) were considered.

5.1 Effectiveness of Ground Improvement on the Design Outcome

Figure 11(a) compares the horizontal deflections computed from analytical and FE methods for different levels of pile length variation. The analytical design predicts a larger variation in the horizontal deflection with vertical improvement than the EP and LE FE models. The analytical design predicted 4.69 mm horizontal deflection for the foundation in unimproved soil, while the EP and LE FE models predicted 2.08 mm and 1.94 mm, respectively. The analytical design predicted a substantial increase in the horizontal deflection with the depth of ground improvement due to the massive reduction in pile length compared to FE models. Also, the LE model showed lower deflections than the EP model, but the difference is small. It must be noted that the moment capacity governed the design in unimproved soil and the differential settlement in the improved soil.

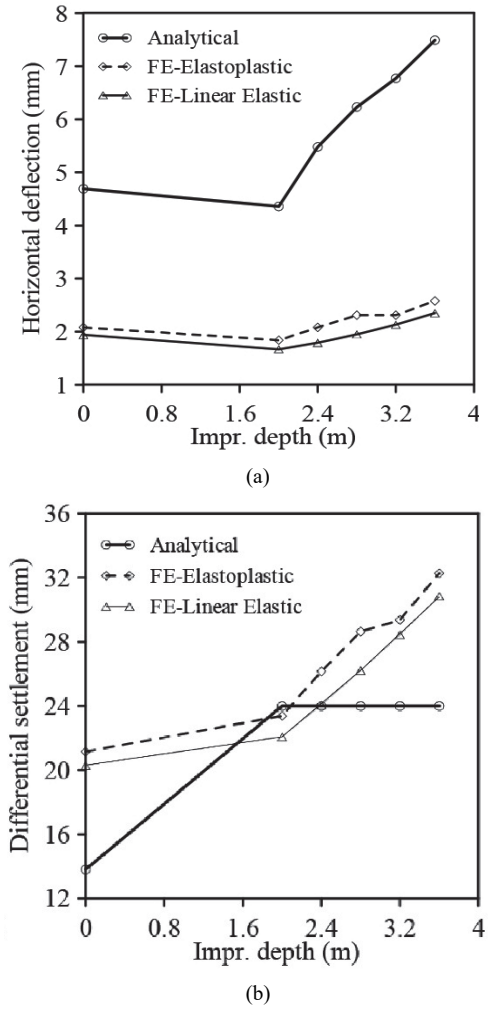

Fig 11 Comparison of analytical and FE analysis results (varying pile length): (a) horizontal deflection and (b) differential settlement

Figure 11(b) compares differential settlements computed from analytical and FE models. The analytical method predicted 13.80 mm differential settlement for unimproved soil and flattened at 24 mm for all the improved cases (design controlled by differential settlement). The differential settlement increased with an increase in improvement levels from the FE results. It must be noted that FE models were created from the analytical design outcome where the pile length was reduced massively with ground improvement to obtain the critical differential settlement of 24 mm. Thus, FE models predicted an increase in the differential settlement with ground improvement because of the reduced length of the pile. The EP model predicts a differential settlement of 21.15 mm for the unimproved soil (L_p = 48.4 m) and 32.28 mm for improvement level V_5 (L_p = 9.85 m). The LE model predicts a differential settlement of 20.29 mm for the unimproved soil (L_p = 48.4 m) and 30.85 mm for improvement level V_5 (L_p = 9.85 m).

5.2 Performance Piled-Raft Foundation with and without Ground Improvement

The performance of the foundation in terms of deflections

was compared for the same geometry of the foundation, as shown in Fig. 12(a). The analytical design predicts the horizontal deflection to be 4.69 mm in the unimproved soil and decrease to 3.10 mm for the improvement level V_5. However, for the FE models, the horizontal deflection decreased from unimproved soil to the first depth of improvement, but the change in horizontal deflection was minimal with the depth of improvement. The EP and the LE models had a similar pattern and smaller horizontal deflection, possibly because the pile's length adopted (48.4 m) was conservative. It is evident that this pile length is not required for the improved soil, as can be seen from Fig. 12(a), where the reduced pile length also yielded acceptable horizontal deflection. The horizontal deflection has almost reached a constant value, where increasing the improvement depth had little effect.

Figure 12(b) compares the results of differential settlements. The analytical design predicted a decrease in the differential settlement with increased ground improvement. The analytical design predicted a differential settlement of 13.80 mm for the unimproved soil and decreased to 12.80 mm with V_5 improvement.

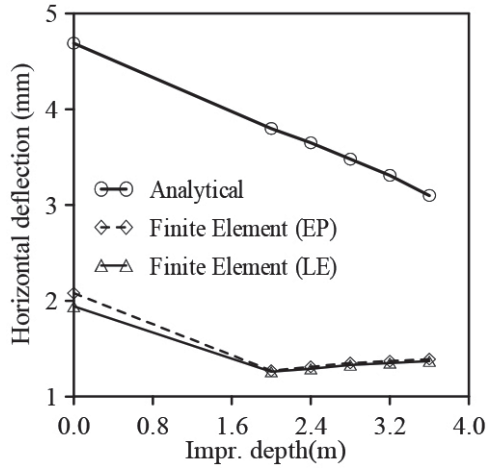

(a)

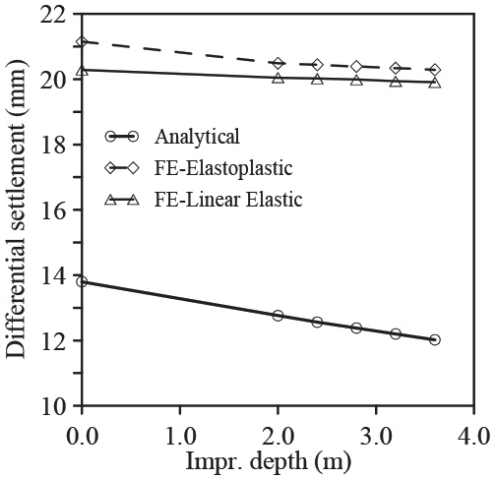

(b)

Fig. 12 Comparison of analytical and FE analysis results (pile length = length of the pile in the unimproved ground) (a) horizontal deflection and (b) differential settlement

The differential settlement for the unimproved soil for the EP-FE model was 21.15 mm and decreased to 20.29 mm for the V_5 improvement level. Similarly. The LE-FE model yielded a differential settlement of 20.29 mm and decreased to 19.97 mm. The decrease from unimproved to improved soil is minimal, and there is a little change with further improvement.

6. EFFECT OF RADIUS OF GROUND IMPROVEMENT ON THE PERFORMANCE

Two cases were analyzed: (1) FE models created for all the ground improvement geometries, V_iH_i (i = 1-5) with the pile lengths corresponding to each V_i obtained from analytical design and (2) FE models created for all the ground improvement geometries, V_iH_i (i = 1-6) with the pile lengths corresponding to unimproved soil. Figure 13 shows the deformed shape of a piled raft foundation of the EP model for V_1H_6 improvement. It can be seen that all piles are in compression due to the vertical load applied to the raft system. The bending moment and lateral load also caused the piled-raft assembly to twist, leading to a higher magnitude of deformation on one side of the piled-raft assembly than on the other. The Mises stress contour in the soil domain and the piled-raft foundation are shown in Fig. 14. There are small differences in Von-Mises stresses, as shown in the figure, but there are minimally higher stress values at the piled-raft interface due to the deformation of the system with the given load.

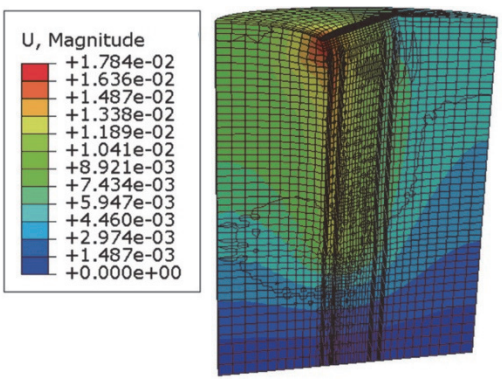

(a)

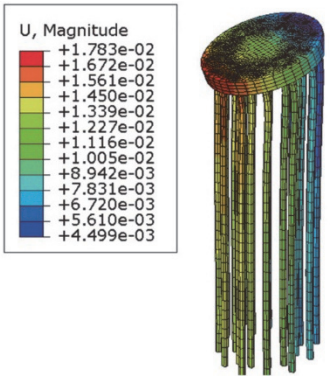

(b)

Fig. 13 Deformed shape of the model with displacement contours (a) a cut section of the simulation domain and (b) piled-raft foundation (deformation scale factor = 200)

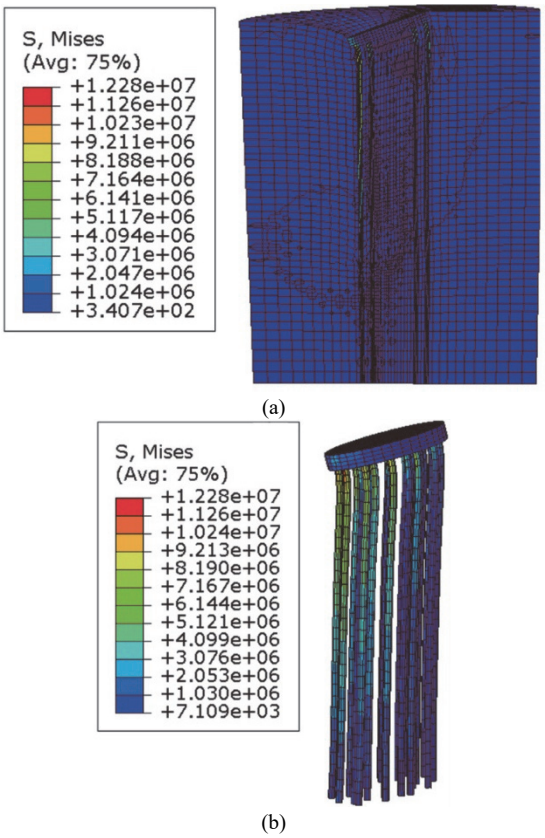

Fig. 14 Von-Mises stress contours (a) cross-section of the simulation domain and (b) piled-raft assembly (deformation scale factor = 200)

6.1 Effectiveness of Ground Improvement on Design Outcomes

The analytical designs only considered the vertical variation in ground improvement, but the FE designs incorporated horizontal and vertical variations. The analysis based on the FE models helps determine the most effective design. Figures 15(a) and 15(b) show the horizontal deflections obtained from LE and EP FE models, respectively. Figure 15(a) reveals the increase in the horizontal deflection from the unimproved case to the first level of ground improvement. Though the horizontal deflection is expected to decrease with improvement, it increases in this case because of the massive reduction in length of the pile; 48.4 m in the unimproved ground to 23.07 m in improved depth V_1. The horizontal deflection increased from 1.94 mm in the unimproved ground to 2.10 mm at V_1. The effect of the decrease in length outweighs the effect of improvement and thus leads to higher deflection. The trend of increase in horizontal deflection with each level of vertical improvement (V_i; i = 0 to 5) can be attributed to the reduction in the length of the pile (48.4 m to 9.85 m).

Keeping the depth of vertical improvement constant and increasing the radius of horizontal improvement led to a decrease in horizontal deflection. For the LE model, the vertical improvement V_5 (L_p = 9.85 m) led to a maximum deflection of 3.36 mm for the radius of horizontal improvement H_1 (6.0 m), and it decreased to 2.32 mm at H_5 (7.6 m). This shows the effect of horizontal improvement on horizontal deflection. The EP model results, as shown in Fig. 15(b), also reveal a similar behavior to that of the LE model. The EP model, however, shows larger deflection values

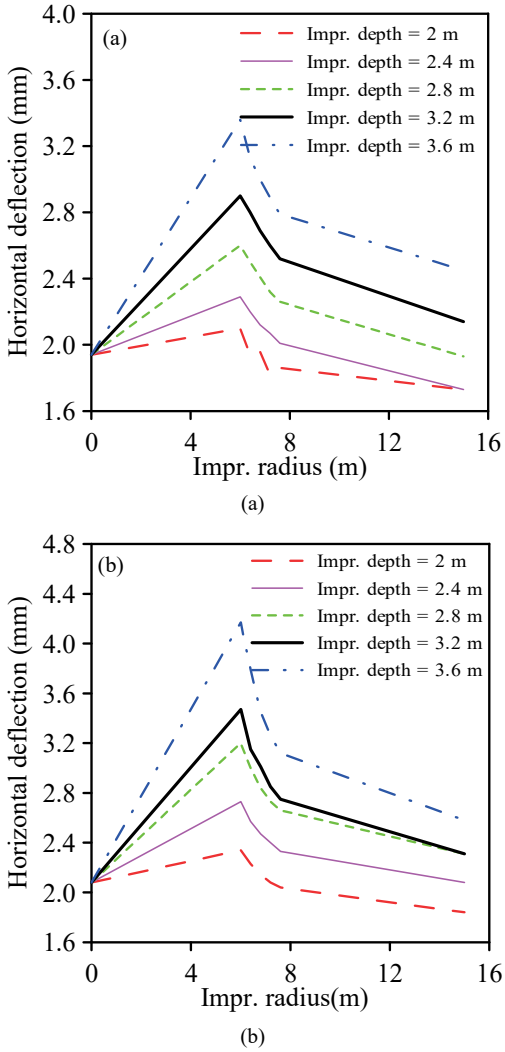

Fig. 15 Variation of horizontal deflection with improvement radius (a) linear elastic model and (b) elastoplastic model

when compared to the LE models with the same case of improvement. In the unimproved case (L_p = 48.4 m), the EP model had a horizontal deflection of 2.08 mm compared to 1.94 mm from the LE model. For the EP model, the vertical improvement V_5 (L_p = 9.85 m) led to a maximum deflection of 4.17 mm at a radius of horizontal improvement H_1 (6.0 m), and it decreased to 2.58 mm at H_5 (7.6 m). The ground improvement yielded acceptable values of horizontal deflection for both EP and LE models, even with a considerable reduction in the length of the pile.

Figures 16 (a) and 16(b) show the differential settlements from LE and EP analyses, respectively. The differential settlement increased with the depth of improvement because of the substantial reduction in the length of piles, which outweighed the effect of depth of improvement. The differential settlement of piled raft in the unimproved ground (L_p = 48.4 m) for the LE model was 20.29 mm, and it increased with an increase in depth of vertical ground improvement. For ground improvement in horizontal direction H_1, the differential settlement increased from 22.31 mm at improvement V_1 to 32.40 mm at improvement V_5. The pile lengths in these two cases were 23.07 m and 9.85 m, respectively.

Unlike the horizontal deflection, the increase in the radius of improvement had little effect on differential settlement. The

increase in differential settlement upon an increase in the radius of ground improvement was small. The LE model with the vertical ground improvement V_5 (L_p = 9.85 m) showed a maximum differential settlement of 32.40 mm for the horizontal improvement H_1 (6.2 m). It decreased to 30.85 mm at H_6 (model boundary = 15 m). This shows that the effect of horizontal improvement on the differential settlement is minimal. Figure 16(b) shows the differential settlement behavior of the EP model with different levels of ground improvement and reveals a similar response to that of the LE model. The values of the differential settlement are higher for EP models than LE models. In the unimproved case (L_p = 48.4 m), the EP model had a differential settlement of 21.15 mm compared to 20.29 mm for the LE model. For the EP model, the vertical improvement V_5 (L_p = 9.85 m) led to a maximum differential settlement of 35.26 mm for horizontal improvement H_1 (6.2 m), and it decreased to 32.28 mm at H_6. Figure 16 shows that the improvement to level V_1 (L_p= 23.07 m) resulted in a differential settlement of 23.78 mm, which is within the allowable limit of 24 mm. Due to the significant reduction in the pile length, the other improvement levels provide differential settlement higher than the permissible limit.

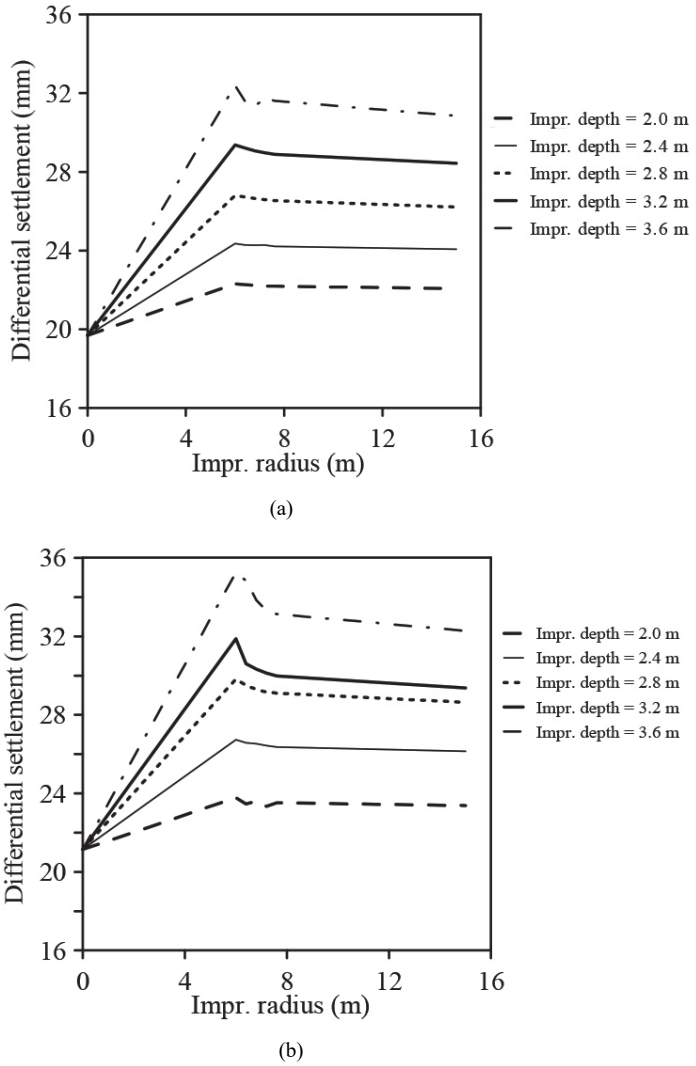

Fig. 16 Variation of differential settlement with ground improvement radius (a) linear elastic model and (b) elasto-plastic model

6.2 Performance Piled-Raft Foundation With and Without Ground Improvement

To understand the performance effect of ground improvement on the performance of piled-raft foundation, 3D FE models were created with the length of the pile needed for the unimproved soil. The dimensions of the piled-raft were fixed, and results on horizontal deflection and differential settlement were obtained by varying the level of ground improvement around the piled raft. Figures 17(a) and 17(b) show the horizontal deflection of the piled raft foundation for different levels of ground improvement when the pile length is fixed at 48.4 m, which is equivalent to that of the unimproved soil. The figure shows a small decrease in horizontal deflection with variation in the radius of ground improvement in the horizontal direction for the same depth of vertical ground improvement. For the LE model, displacement decreases from 1.94 mm in the unimproved case (L_p = 48.4 m) to 1.82 mm for improvement H_1 (6.0 m) and 1.37 mm at H_6 (model boundary = 15 m) when vertical improvement is V_5 (L_p = 48.4 m). Similarly, for the EP model, displacement decreases from 2.08 mm in the unimproved soil (L_p = 48.4 m) to 1.85 mm for improvement H_1 (6.0 m)

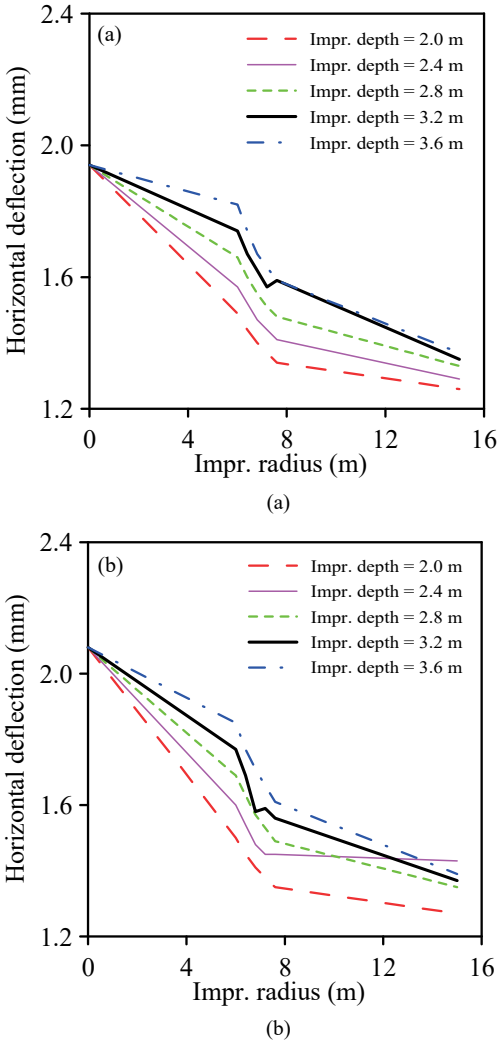

Fig. 17 Variation of horizontal deflection with ground improvement radius (pile length = length of the pile in the unimproved ground): (a) linear elastic model and (b) elasto-plastic model

and 1.39 mm at H_6 (model boundary = 15 m) when vertical improvement is V_5 (L_p = 48.4 m). The horizontal deflection increases slightly with the increase in depth of improvement and is in the range of 10^{-2} mm. This unusual behavior can be due to the complex interaction between the soil-raft, raft-pile, and soil-pile. The pile length adopted from the analytical design was very conservative and yielded a minimal horizontal deflection of 1.94 mm in the unimproved ground. This value is minimal compared to the allowable horizontal deflection. Thus, improving the ground with the length of piles intact does not yield considerable improvement in the deformation behavior of the piled-raft as the deformation is already minimal.

The differential settlement slightly decreased with ground improvement. For the LE model, as shown in Fig. 18(a), the differential settlement decreased from 20.29 mm in unimproved case (L_p = 48.4) m to a minimum deflection of 19.91 mm when improved vertically to V_5 (L_p = 48.4 m) and horizontal improvement to the boundary of the model (H_6). There is minimal or no decrease in the differential settlement with the increase in horizontal improvement (H_1 to H_6) when the depth of vertical improvement is kept constant. The case is similar to the EP model, as seen in Fig. 18(b). The differential settlement decreases from 21.15 mm in the unimproved case (L_p = 48.4 m) to a minimum deflection of 20.29 mm when improved to vertical level V_5 (L_p = 48.4 m) with the horizontal improvement extending to the boundary of the model (H_6). The differential settlement decreases with the increase in the depth of vertical improvement, but the decrease is very small.

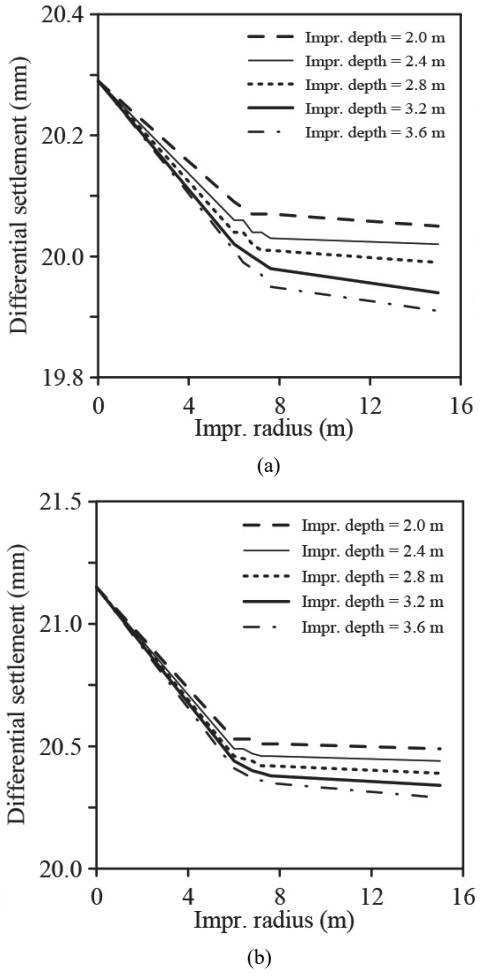

Fig. 18 Variation of differential settlement with ground improvement radius (pile length = length of the pile in the unimproved ground): (a) linear elastic and (b) elasto-plastic

7. PARAMETRIC STUDIES: EFFECT OF VARIATION IN SOIL PROPERTIES

The results presented in the previous sections are based on the mean soil properties. Therefore, a parametric study in unimproved and improved soils was performed by changing the value of undrained shear strength (c_u). In both improved and unimproved soils, the undrained shear strength was varied using a coefficient of variance (COV) of 20 %. The mean undrained shear strength (μ) was 41 kPa with a standard deviation (σ) of 8.2 kPa in the case of unimproved soil. Likewise, the improved soil's mean shear strength was 360 kPa, and the standard deviation was 72 kPa. Although a ±3σ is used in probabilistic analyses for considering possible variations, only ±1σ was considered in this study. The variation of c_u for the soil profile improved to level V_5 is shown in Fig. 19.

Figure 20 shows a similar variation but for the FE models. The FE analysis results show that for the unimproved case, the variation of c_u did not influence the horizontal deflection. The horizontal deflection value is predominantly small (1.94 mm) for the mean cohesion value with the length (48.4 m). The result from the FE design has the same pattern as that of the analytical design, but the magnitude of deflection obtained from the FE design results is slightly smaller.

Similarly, the effect of variation of c_u on the differential settlement behavior for analytical design and FE models was investigated. Figure 21 shows the results from the analytical design on differential settlement due to variation in c_u. For the mean c_u, the differential settlement is 13.80 mm in the unimproved case and 24 mm for the improved cases. Differential settlement controls for the design in improved cases. When the c_u decreased from the mean, the differential settlement increased, and vice-versa when the c_u increased from the mean. For negative deviation in c_u (μ – 1σ), the differential settlement grew from 16.82 mm in the unimproved case (L_p = 48.4 m) to 30.28 mm for the first level of ground improvement V_1 (L_p = 19.75 m). It decreased with further improvement leading to a value of 25.54 mm for V_5 (L_p = 9.85 m). For

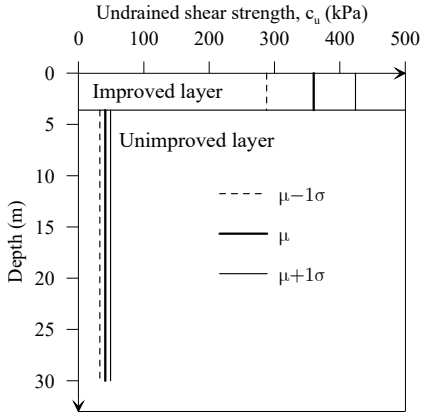

Fig. 19 Variation of undrained shear strength of improved and unimproved soil profile for parametric study (for improvement depth of V_5)

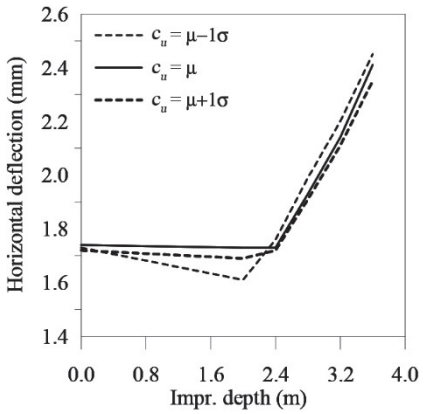

Fig. 20 Effect of variation in undrained shear strength of unimproved grounds on horizontal deflection from FE analysis

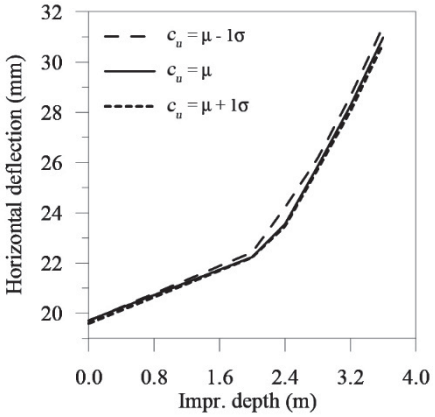

Fig. 22 Effect of variation in undrained shear strength of unimproved grounds on differential settlement from FE analyses

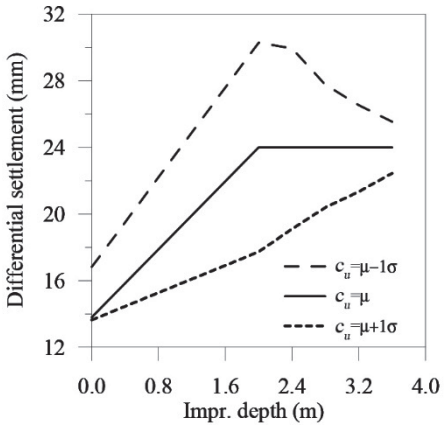

Fig. 21 Effect of variation in undrained shear strength of unimproved and improved grounds on differential settlement from analytical calculations

positive deviation in c_u ($\mu + 1\sigma$), the differential settlement increased from 13.64 mm in the unimproved case (L_p = 48.4) to 17.73 mm for the first level of improvement V_1 (L_p = 19.75 m). It increased with further improvement leading to a value of 22.24 mm for the improvement V_5 (L_p = 9.85 m). The difference in the pattern for positive and negative deviations is due to the ground improvement decreasing the settlement in soil with lower strength.

Figure 22 shows the results of differential settlement due to the variation in c_u for the FE models. The FE results show that for the unimproved case, the variation of c_u did not influence the differential settlement. The horizontal deflection value is approximately 19.7 mm and does not change with the variation in mean cohesion when the pile length is kept constant at 48.4 m. The differential settlement increases with ground improvement due to the decrease in pile length, outweighing the effect of ground improvement. The models with higher c_u values have a lower differential settlement, as seen in Fig. 22. The difference in the differential settlement between the mean and the negative and positive deviations from the mean is minimal. The differential settlement for improvement level V_5 for $\mu - 1\sigma$, μ, and $\mu + 1\sigma$ values of c_u are 31.42, 30.97, and 30.73 mm, respectively.

8. NET COST-BENEFIT WITH THE DEPTH OF GROUND IMPROVEMENT

Generally, the cost of a wind turbine is concerned with the cost of the structure itself, namely the electrical, mechanical, and structural components. However, the cost of the foundation and the effect of the subsurface properties should be considered for this study as the foundations are large for taller wind turbines, and the ground has been modified to enhance the weak subsurface soil properties. The unit cost of the piled-raft foundation construction, including material, labor, and equipment costs and cost of ground improvement, were obtained from the widely used estimating book RS Means Building construction cost data (Weaver and Charest 2013).

The net economic benefit, the difference between the total cost of the foundation in unimproved ground and in the improved ground, of constructing a piled-raft foundation for the five depths of ground improvement is shown in Fig. 23(a). Figure 23(a) shows that the total cost of the piled-raft foundation in the unimproved ground is higher than all levels of improved soil, which indicates that improving the near-surface soil can create a net economic advantage. The results show that the cost-benefit was the highest when the ground was improved to a depth of 2 m (V_1) and 3.6 m (V_5). The former yielded a saving of $70,585, and the latter yielded a saving of $65,247. The maximum cost-benefit of $72,342 was predicted when the ground was improved to a depth of 2.4 m, which had the most economical balance of the cost of the depth of ground improvement and the length of piles. These results clearly show the benefit of modifying the ground, although the cost-benefit has more significance as more wind turbines are built on a wind farm.

A parametric study was conducted to investigate the effects of modulus of undrained shear strength of insitu and improved soils on the design outcomes and net economic advantages. The insitu soil has a mean undrained shear strength (μ) of 41 kPa and a standard deviation (σ) of 8.2 kPa. Similarly, the improved soil has a mean undrained shear strength of 360 kPa and a standard deviation of 72 kPa. For the parametric study, the undrained shear strength was varied by $\pm 1\sigma$ for both insitu and improved soils to compare total costs. The total construction costs of the piled-raft foundations with a variation in shear strength of the soil as the

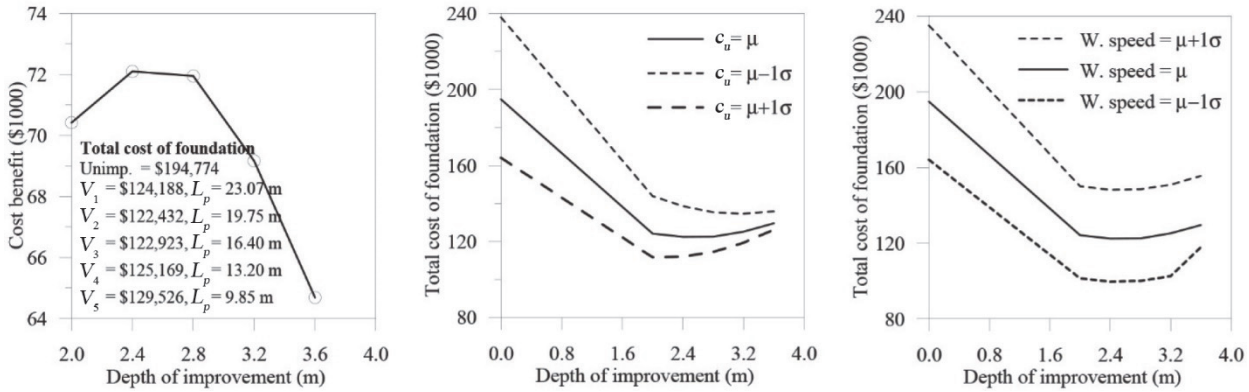

Fig. 23 Variation of (a) cost-benefit, (b) total cost of foundation for different values of undrained shear strength of soil, and (c) total cost of foundation for different wind speeds vs. depth of ground improvement

length of the pile (L_p) varies to meet the required design requirements for all the cases are presented in Fig. 23(b). The pile length necessary to meet the design requirements varies with both the undrained shear strength and the depth of ground improvement. It can be seen that there is a significant reduction in the total cost from insitu to the first depth of improvement (V_1) and a slight increase in total cost for other depths of improvement. There is an increase in cost for the $\mu - 1\sigma$ for both insitu and all the depths of improved soils and a decrease in cost for $\mu + 1\sigma$ cases, which is related to the length of the piles. For all the cases of ground improvement, the construction is economical and can result in a net cost saving.

Another parametric study was conducted to investigate the effects of wind speed variation on the design outcomes and cost-benefit. A change in wind speed changes the horizontal load and bending moment at the base of the tower, which accounts for variation in the height of the wind turbine tower indirectly because the wind speed is higher at higher altitudes. This study assumed a standard deviation (σ) of 8 mph for the mean wind speed (μ) of 80 mph. The parametric study was conducted by varying wind speed by $\pm 1\sigma$. The corresponding total costs were computed for insitu and all the depths of improved cases. Further, the comparison of the total construction costs of the piled-raft foundation for various wind speeds is summarized in Fig. 23(c). The figure shows the total construction cost of the foundation with and without ground improvement for all cases of the parametric study. Overall, the maximum cost of the piled-raft foundation is for the higher wind speeds ($\mu + 1\sigma$), and the minimum cost is for the lower wind speeds ($\mu - 1\sigma$) for the unimproved and improved cases. A significant reduction in the cost can be seen from the unimproved case to the first and second levels of improvement (V_1 and V_2) for all the wind speed values. However, the total cost increases for the improvement beyond V_2, which makes it the least costly.

9. CONCLUSIONS

It was found from the analytical procedure that the safety criterion (moment capacity) governed the design of piled raft foundation in unimproved soil and the serviceability criterion (differential settlement) in the improved soil. It was also found that a significant reduction in the pile length could be achieved by improving the near-surface soil while meeting the safety and serviceability criteria. A comparison of analytical and FE analysis results with optimal design (varying pile length) showed that the horizontal deflection was over-predicted by the analytical procedures. Although elastic and elastoplastic models predicted similar horizontal deflection, the elastoplastic model predicted a slightly higher horizontal deflection. On the other hand, the analytical procedure underpredicted the differential settlement. A similar trend was observed for analysis, with the pile length equal to the length required to meet the design requirement in unimproved soil. Cost analysis results show that improving the near-surface soil can produce a net economic advantage. The results show that the cost-benefit was the highest when the ground was improved to a depth of 2 m (V_1) and 3.6 m (V_5).

FUNDING

The authors received no funding for this work.

DATA AVAILABILITY

All data, models, and code generated or used during the study appear in the submitted article.

CONFLICT OF INTEREST STATEMENT

The authors declare that there is no conflict of interest.

REFERENCES

ASCE. (2010). *Minimum Design Loads for Buildings and Other Structures*. *ASCE/SEI Standard 7-10*. American Society of Civil Engineers, 187-297.

Bourgeois, E., Hassen, G., and Buhan, P. (2011). "Finite element simulations of the behavior of piled-raft foundationsusing a multiphase model," *International Journal for Numerical and Analytical Methods in Geomechanics*, **37**(9), 1122-1139. https://doi.org/10.1002/nag.2077

Brom's, B.B. (1964a). "Lateral resistance of piles in cohesive soils." *Journal of the Soil Mechanics and Foundation Division,* American Society of Civil Engineers, ASCE, **90**, 27-63.

Clancy, P. and Randolph, M.F. (1993). "An approximate analysis procedure for analysis of piled raft foundations." *International Journal for Numerical and Analytical Methods in Geomechanics.* https://doi.org/10.1002/nag.1610171203

Fellenius, B.H. (1999). *Basics of Foundation Design*, 2nd Ed., BiTech Publishers, Richmond, British Columbia.

Gaihre, N. (2020). *Analytical and Numerical Modeling of Foundations for Tall Wind Turbine in Various Soils*. M.S. Thesis, Department of Civil and Environmental Engineering, Southern Illinois University, Carbondale, USA.

Grunberg, J. and Gohlmann, J. (2013). *Concrete Structures for Wind Turbines*. Wilhelm Ernst & Sohn, Berlin, Germany, ISBN 978-3-433-03041-7.

Lantz, E., Roberts, O., Nunemaker, J., Demeo, E., Dykes, K., and Scott, G. (2019). *Increasing Wind Turbine Tower Heights: Opportunities and Challenges*, National Renewable Energy Laboratory, Golden, CO, NREL/TP-5000-73629.

Lyrner, T., Hassanzadeh, M., Stalin, T., and Johansson, J. (2010). *Tall Towers for Large Wind Turbines*, Report from Vindforsk Project V-342 Höga.

Melese, F. (2022). "Improved performance of raft foundation using detached pile columns in loose subsoil conditions." *Advances in Civil Engineering*, **18**. https://doi.org/10.1155/2022/4002545

NFEC. (1986). *DM-7.02 Foundation and Earth Structures.* Alexandria, VA.

O'Neill, M.W. and Reese, L.C. (1999). *Drilled Shafts: Construction Procedures and Design Methods*, Publication FHwA-IF-99-025, FHwA, Washington, DC.

Pham, H.V., Dias, D., Miranda, T., Cristelo, N., and Araújo, N. (2018). "3D Numerical modeling of foundation solutions for wind turbines." *International Journal of Geomechanics*, **18**(12), 86-99. https://doi.org/10.1061/(asce)gm.1943-5622.0001318

Quiroga, A.J., Thompson, Z.M., Muraleetharan, K.K., Miller, G.A., and Cerato, A.B. (2017). "Stress-strain behavior of cement-improved clays: Testing and modeling." *Acta Geotechnica*, Springer Berlin Heidelberg, **12**(5), 1003-1020.

Randolph, M. F. (1994). "Design methods for pile groups and piled-rafts." *13th International Conference on Soil Mechanics and Foundation Engineering*, New Delhi, India, 61-82.

Ravichandran, N. and Shrestha, S. (2018). "Performance and cost-based robust design optimization procedure for typical foundations for wind turbine." *International Journal of Geotechnical Engineering*, 1-14.

Shrestha, S. and Ravichandran, N. (2017). "Geotechnical design and design optimization of pile-raft foundation for tall onshore wind turbines in multi-layered clay." *International Journal of Geomechanics*, ASCE, **18**(2). https://doi.org/10.1061/(ASCE)GM.1943-5622.0001061

Taghavi, A., Muraleetharan, K.K., Miller, G.A., and Cerato, A.B. (2015). "Centrifuge modeling of laterally loaded pile groups in improved soft clay." *Journal of Geotechnical and Geoenvironmental Engineering*, **142**(4), 04015099.

Weaver, J.F. (2017). *World's Tallest Wind Turbine Built in Germany*. Electrek. https://electrek.co/2017/11/02/worlds-tallest-wind-turbine-built-in-germany/

Yamashita, K., Hamada, J., Onimaru, S., and Higashino, M. (2012). "Seismic behavior of piled-raft with ground improvement supporting a base-isolated building on soft ground in Tokyo." *Soils and Foundations*, Elsevier, **52**(5), 1000-1015.